Eur. Phys. J. C 23, 259–266 (2002)
Digital Object Identifier (DOI) 10.1007/s100520100868

THE EUROPEAN PHYSICAL JOURNAL C

Comparison of phase space slicing and dipole subtraction methods for $\gamma^* \to Q\bar{Q}$

T.O. Eynck[1], E. Laenen[1], L. Phaf[1], S. Weinzierl[2]

[1] NIKHEF Theory Group, Kruislaan 409, 1098 SJ Amsterdam, The Netherlands
[2] Dipartimento di Fisica, Università di Parma, INFN Gruppo Collegato di Parma, 43100 Parma, Italy

Received: 15 October 2001 /
Published online: 25 January 2002 –

Abstract. We compare the phase space slicing and dipole subtraction methods in the computation of the inclusive and differential next-to-leading order cross sections for heavy quark production in the simple process $\gamma^* \to Q\bar{Q}$. For the phase space slicing method we study the effects of improvement terms that remove restrictions on the slicing parameter $s_{\min}$. For the dipole method our comparison is a first check on some of its counterterms involving massive quarks, derived recently. In our comparison we address issues such as numerical accuracy and efficiency.

1 Introduction

Fully differential QCD cross sections are important observables for studies at high-energy colliders. By allowing detector-specific acceptance cuts on phase space variables they eliminate the need for extrapolation into unmeasured, and often also poorly calculable regions, and thereby improve theory–experiment comparisons. Reliable theoretical predictions for such differential cross sections require the inclusion of at least next-to-leading order (NLO) QCD corrections. NLO calculations combine virtual one-loop corrections with the real emission contributions from unresolved partons. These two parts are usually computed separately and each is infrared divergent; only their sum is infrared finite. NLO Monte-Carlo programs incorporate both pieces and allow the simultaneous computation of many differential cross sections for the particular reaction considered.

However, these programs require that infrared singularities be eliminated before any numerical integration can be done. There are essentially two types of methods to effect this cancellation. The phase space slicing (PSS) method [1–4] is based on approximating the matrix elements and the phase space integration measure in boundary regions of phase space so integration may be carried out analytically. The subtraction method [5–7] is based on adding and subtracting counter terms designed to approximate the real emission amplitudes in the phase space boundary regions on the one hand, and to be integrable with respect to the momentum of an unresolved parton.

For massless partons both methods are well developed and have been widely used. A quite general formulation of phase space slicing has been given in [8,9]. It was extended to include massive quarks and identified hadrons in [10].

There exist two general formulations of the subtraction method. One is the residue approach [11], the other the dipole formalism [12]. Both can handle massless partons and identified hadrons in the final and/or initial state. The extension of the dipole method to handle massive quarks, using dimensional regularization, has been given recently in [13]. An extension to photon radiation off massive fermions, using small masses for infrared regularization, was developed by Dittmaier in [14]. There are also hybrid methods [15] that combine elements of the slicing and subtraction methods such that both the resolved and unresolved contributions are numerically small and can be reliably integrated.

With general formulations of the phase space slicing and dipole methods for massless and massive quarks now available, it is interesting to compare their efficiency and accuracy. In this paper we do this for (differential) "cross sections" for heavy quark production in the process $\gamma^* \to Q\bar{Q}$. This case is of course very simple but also generic for more complicated processes. In the case of the NLO cross section for $t\bar{t}H$ production [16,17] it was recently verified [17] that the slicing method and a somewhat differently phrased dipole method [18] agreed.

Our results using the dipole subtraction method represent the first numerical implementation of some of the subtraction terms computed in [13]. While the dipole method is exact, the PSS method requires the introduction of a theoretical resolution parameter $s_{\min}$, usually required to be quite small. We include improvement terms in the PSS method [19], and study their effect of removing restrictions on the size of the phase space slicing cut-off. This is especially important for cross sections involving heavy quark production, and allows for a free choice of slicing parameter without reference to the heavy quark mass, a

prerequisite for considering the high-energy or zero-mass limit.

This paper is structured as follows. In Sect. 2 we compute the fully differential cross section for $\gamma^* \to Q\bar{Q}$ using the PSS method, including the improvement terms. In Sect. 3 we compute this cross section with the dipole subtraction method. In Sect. 4 we present a numerical comparison of the two methods, followed by our conclusions.

2 Phase space slicing

We consider the process

$$\gamma^*(q) \to Q(p_1) + \bar{Q}(p_2), \tag{1}$$

with $p_1^2 = p_2^2 = m^2$. The NLO corrections involve virtual corrections to (1) and the gluon bremsstrahlung reaction

$$\gamma^*(q) \to Q(p_1) + \bar{Q}(p_2) + g(p_3), \tag{2}$$

with $p_3^2 = 0$. We define the invariants

$$s_{ij} \equiv 2p_i \cdot p_j, \quad \tilde{s}_{ij} \equiv (p_i + p_j)^2 . \tag{3}$$

The final state phase space for the 3-parton contribution is divided into "hard" and "soft" regions. The hard region, in which all 3 final state particles in (1) are resolved, is defined such that $s_{13} > s_{\min}$ or $s_{23} > s_{\min}$. (In an appendix we discuss this definition when more than one color structure is present.) The complementary region is soft. Let us review the approximations involved in PSS, following [19]. The 3-parton contribution to the fully differential decay can be written schematically as

$$\begin{aligned} \mathrm{d}\Gamma_3 &= |\mathcal{M}_3|^2 \times \mathrm{dPS}_3 \\ &= \left(|\mathcal{M}_3|^2 \times (1-\theta_s) + |\mathcal{M}_3|^2 \times \theta_s\right) \times \mathrm{dPS}_3 \\ &= |\mathcal{M}_3|^2 \times (1-\theta_s)\mathrm{dPS}_3 \\ &\quad + \theta_s \times \left(T_1(\theta_s) + T_2(\theta_s) + T_3(\theta_s)\right), \end{aligned} \tag{4}$$

where $|\mathcal{M}_3|^2$ is the exact matrix element squared, and dPS_3 denotes the exact 3-particle phase space measure. Note that we do not consider the effect of jet-algorithms here (they are implicit in the definition of the phase space). The slicing of phase space is indicated by the symbol θ_s, which is 0 in the hard phase space region and 1 in the soft region. T_1 is given by

$$\begin{aligned} T_1(\theta_s) &= S|\mathcal{M}_2|^2 \times \mathrm{dPS}_{\mathrm{soft}}\ \mathrm{dPS}_2 \\ &= R(\theta_s)|\mathcal{M}_2|^2 \times \mathrm{dPS}_2\ , \end{aligned} \tag{5}$$

and represents the integral of the approximate matrix element $|\mathcal{M}_3|^2 \to S|\mathcal{M}_2|^2$ over the approximate phase space $\mathrm{dPS}_3 \to \mathrm{dPS}_{\mathrm{soft}}\mathrm{dPS}_2$. The resolution factor $R(\theta_s)$ is independent of the hard scattering and can be calculated analytically for a wide range of multiparton processes [8–10]. T_2 is given by

$$T_2(\theta_s) = \left(|\mathcal{M}_3|^2 - S|\mathcal{M}_2|^2\right) \times \mathrm{dPS}_3, \tag{6}$$

and represents the integral over the exact 3-particle phase space of the difference between the true matrix element and the approximate matrix element. T_3 is given by

$$T_3(\theta_s) = S|\mathcal{M}_2|^2 \left(\mathrm{dPS}_3 - \mathrm{dPS}_2\mathrm{dPS}_{\mathrm{soft}}\right), \tag{7}$$

and represents the difference between the integrals of the approximate matrix element over the true and approximate unresolved phase space. Note that T_1 contains the soft and collinear divergences needed to cancel the singularities of the virtual term, while T_2 and T_3 are finite and vanish as the domain of support for θ_s is taken to zero.

2.1 Matrix element

The matrix elements for the NLO cross section for process (1) are not very complicated, so we can be explicit. At lowest order we have

$$\begin{aligned} \mathrm{d}\Gamma_2 &= \frac{1}{3}\frac{1}{2\sqrt{s}} N e_q^2 e^2 \left(8m^2 + 4s\right) \mathrm{dPS}_2 \\ &= \frac{1}{3}\frac{1}{2\sqrt{s}} \left|\mathcal{M}_{\mathrm{Born}}\right|^2 \mathrm{dPS}_2, \end{aligned} \tag{8}$$

where N is the number of colors, e_q the fraction of the elementary charge e of the heavy quark, m its mass, $s = q^2$ and

$$\mathrm{dPS}_2 = \frac{1}{(2\pi)^2}\frac{\mathrm{d}^3p_1}{2E_1}\frac{\mathrm{d}^3p_2}{2E_2}\delta^{(4)}(q - p_1 - p_2). \tag{9}$$

Note that in NLO approximation $|\mathcal{M}_2|^2$ in (5) is $|\mathcal{M}_{\mathrm{Born}}|^2$. At $\mathcal{O}(\alpha_s)$ there are virtual and real emission contributions. The PSS method separates the latter into hard and soft contributions. The (spin- and color-summed) matrix element for the real emission process (2) is

$$|\mathcal{M}_3|^2 = 16 e_q^2 e^2 g_s^2 N C_F I_R, \tag{10}$$

with g_s the strong coupling, $C_F = (N^2-1)/2N$ and

$$\begin{aligned} I_R = &-\frac{m^2 s_{23}}{s_{13}^2} - \frac{m^2 s_{12}}{s_{13}^2} - \frac{4m^4}{s_{13}^2} + \frac{4m^2 s_{12}}{s_{13}s_{23}} + \frac{s_{12}^2}{s_{13}s_{23}} \\ &+ \frac{s_{23}}{2s_{13}} + \frac{s_{12}}{s_{13}} - \frac{m^2}{s_{13}} - \frac{m^2 s_{13}}{s_{23}^2} + \frac{s_{13}}{2s_{23}} - \frac{m^2 s_{12}}{s_{23}^2} \\ &- \frac{4m^4}{s_{23}^2} + \frac{s_{12}}{s_{23}} - \frac{m^2}{s_{23}}. \end{aligned} \tag{11}$$

In the T_1 term (5) the eikonal approximation of the exact matrix element is used. The integral over $\mathrm{dPS}_{\mathrm{soft}}$ is then performed analytically and added to the virtual corrections. The approximated matrix element in the soft region (5) is

$$S\left|\mathcal{M}_2\right|^2 = 16 e_q^2 e^2 g_s^2 N C_F I_S, \tag{12}$$

where

$$I_S = -\frac{m^2 s_{12}}{s_{13}^2} + \frac{4m^2 s_{12}}{s_{13}s_{23}} - \frac{m^2 s_{12}}{s_{23}^2} - \frac{4m^4}{s_{13}^2} - \frac{4m^4}{s_{23}^2} + \frac{s_{12}^2}{s_{13}s_{23}}. \tag{13}$$

Note that the difference of (11) and (13) which enters the T_2 term (6), is finite in the limit $s_{13}, s_{23} \to 0$.

The result of integrating (12) over $\mathrm{dPS}_{\mathrm{soft}}$ is given in [10], and when added to the virtual contributions, gives the following finite expression for the 2-particle $\mathcal{O}(\alpha_\mathrm{s})$ differential cross section for process (1)

$$\mathrm{d}\Gamma_2 = \frac{1}{3}\frac{1}{2\sqrt{s}}\left(|\mathcal{M}|^2_{\mathrm{soft}} + |\mathcal{M}|^2_{\mathrm{virt}}\right)\mathrm{dPS}_2, \tag{14}$$

with

$$\begin{aligned}
|\mathcal{M}|^2_{\mathrm{soft}} = {} & \frac{\alpha_\mathrm{s} C_F}{\pi} \\
& \times \left[\frac{1}{\epsilon}\left(1+\left(1-\frac{2m^2}{s}\right)\frac{\ln x}{\beta}\right)\right] C_\epsilon \left|\mathcal{M}_{\mathrm{Born}}\right|^2 \\
& + \frac{\alpha_\mathrm{s} C_F}{\pi}\left[-2\left(1+\left(1-\frac{2m^2}{s}\right)\frac{\ln x}{\beta}\right)\right. \\
& \times \left(\ln x - \ln\left(\frac{s}{s_{\min}}\right) - \ln\beta\right) \\
& - 2\left(\ln(1-x) + \ln(1+x) - \ln x\right) + 1 \\
& - \frac{\ln x}{\beta}\left(1-\frac{2m^2}{s}\right)\left(1+2\ln\frac{(1-x)(1+x)}{x}\right) \\
& + \frac{1}{2\beta}\left(1-\frac{2m^2}{s}\right)\left(\mathrm{Li}_2\left(1-\frac{1}{x^2}\right) - \mathrm{Li}_2\left(1-x^2\right)\right) \\
& - \beta + \frac{m^2}{s\beta}\ln x\left(\frac{1-x^2}{x} + \frac{s}{m^2}\left(1-\frac{2m^2}{s}\right)\ln x\right) \\
& \left. + \frac{\ln^2 x}{2\beta}\left(1-\frac{2m^2}{s}\right).\right] \left|\mathcal{M}_{\mathrm{Born}}\right|^2 \\
& + \frac{\alpha_\mathrm{s} C_F}{\pi} N e_q^2 e^2 \left[\left(1+\left(1-\frac{2m^2}{s}\right)\frac{\ln x}{\beta}\right)(-4s)\right]
\end{aligned} \tag{15}$$

and

$$\begin{aligned}
|\mathcal{M}|^2_{\mathrm{virt}} = {} & -\frac{\alpha_\mathrm{s} C_F}{\pi} \\
& \times \left[\frac{1}{\epsilon}\left(1+\left(1-\frac{2m^2}{s}\right)\frac{\ln x}{\beta}\right)\right] C_\epsilon \left|\mathcal{M}_{\mathrm{Born}}\right|^2 \\
& + \frac{\alpha_\mathrm{s} C_F}{\pi} N e_q^2 e^2 \\
& \times \left[-4s - 16m^2 - \frac{m^4}{s\beta}\left(32\mathrm{Li}_2(x) + 64\zeta_2\right)\right. \\
& + \frac{s}{\beta}\left(8\mathrm{Li}_2(x) + 16\zeta_2\right) + \frac{1}{\beta}\ln^2(x)\left(8\frac{m^4}{s} - 2s\right) \\
& - \beta\ln x\left(6s + 8m^2\right) \\
& + \frac{\ln x}{\beta}\left(-32\frac{m^4}{s}\ln(1-x) + 8s\ln(1-x)\right. \\
& \left.\left. + 4s - 8m^2\right)\right].
\end{aligned} \tag{16}$$

Here $C_\epsilon = (4\pi\mu^2/m^2)^\epsilon/\Gamma(1-\epsilon)$, $\beta = (1-4m^2/s)^{1/2}$ and $x = (1-\beta)/(1+\beta)$. We have written the divergent contributions explicitly, even though they cancel between the soft and virtual contribution, so that the method independent (virtual) and method dependent (soft) terms can be easily read off. In particular we can obtain the results within the dipole method by replacing the soft contribution with the integrated dipole terms. Note the logarithmic dependence on the slicing parameter $s_{\min}$ in the finite soft contribution.

2.2 Phase space

The spin-summed squared matrix elements of the previous section are functions of the final state momenta only via the invariants s_{12}, s_{13}, s_{23}. The exact 3-particle phase space

$$\mathrm{dPS}_3 = \frac{1}{(2\pi)^5}\frac{\mathrm{d}^3p_1}{2E_1}\frac{\mathrm{d}^3p_2}{2E_2}\frac{\mathrm{d}^3p_3}{2E_3}\delta^{(4)}(q-p_1-p_2-p_3) \tag{17}$$

may be parametrized in terms of these invariants (after integrating over all remaining variables)

$$\begin{aligned}
\mathrm{dPS}_3 = {} & \frac{1}{4s}\frac{1}{32\pi^3}\mathrm{d}s_{12}\mathrm{d}s_{13}\mathrm{d}s_{23} \\
& \times \delta(s - s_{12} - s_{13} - s_{23} - 2m^2).
\end{aligned} \tag{18}$$

The integration limits of s_{23} at fixed s_{13} are

$$\begin{aligned}
s_{23}^{\pm} = {} & \frac{1}{2\left(s_{13}+m^2\right)}\left(-s_{13}\left(s_{13}-s+2m^2\right)\right. \\
& \left. \pm s_{13}\sqrt{s_{13}^2 - 2s_{13}s - 4sm^2 + s^2}\right).
\end{aligned} \tag{19}$$

The limits of s_{13} at fixed s_{23} are found by exchanging the indices 13 and 23. Setting $s_{23}^{+} = s_{23}^{-}$ we find the maxima of these two invariants

$$s_{13}^{\max} = s_{23}^{\max} = s - 2m\sqrt{s}. \tag{20}$$

In the soft (eikonal) approximation, the limits for s_{23} simplify to

$$\begin{aligned}
s_{23}^{\pm,\mathrm{eik}} = {} & \frac{1}{2m^2}\left(-s_{13}\left(2m^2-s\right) \pm s_{13}\sqrt{s^2-4sm^2}\right) \\
= {} & s_{13}\left(\frac{s-2m^2}{2m^2} \pm \frac{s}{2m^2}\beta\right).
\end{aligned} \tag{21}$$

The phase space boundaries for the exact and approximate cases are given by the Dalitz plot in Fig. 1.

2.3 Results for PSS

We now show some results for the fully inclusive cross section, as well as some differential distributions for process (1). We study what effect including the T_i contributions has on the $s_{\min}$ dependence of the results, and shall see that including all T_i removes all $s_{\min}$ dependence. We use as default values $s = 400\,\mathrm{GeV}^2$, and $m = 5\,\mathrm{GeV}$. Figure 2a

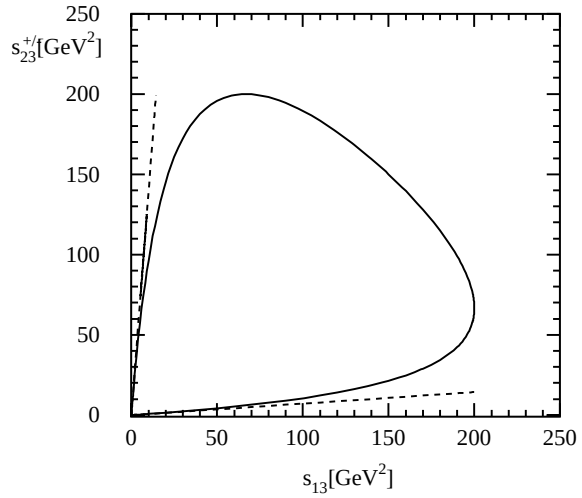

Fig. 1. Dalitz plot for $s_{23}^{\pm}$ as a function of s_{13} for exact (19), solid, and eikonal (21), dashed, phase space boundaries at $m = 5\,\mathrm{GeV}$ and $s = 400\,\mathrm{GeV}^2$

shows that, for the inclusive cross section, not including all T_i leads to $s_{\min}$ dependence (in fact the T_2 worsens the $s_{\min}$ dependence slightly here), but including T_2 and T_3 relaxes all constraints on this parameter. This, however, comes at the expense of potentially lower numerical accuracy, particularly for the differential distributions to be considered below. The inclusion of the T_3 term in particular requires a larger number of points in the Monte Carlo integration than using T_1 alone, to achieve a given accuracy. In practice, therefore, it is common to use only the T_1 in a PSS calculation, with an $s_{\min}$ value small enough for the combined $T_2 + T_3$ contribution to be negligible. One must however be careful not to choose $s_{\min}$ so small that numerical inaccuracies result from the large opposite sign soft + virtual and real emission contributions, as illustrated by Fig. 2b.

Turning to distributions, we show in Fig. 3 the single heavy quark transverse momentum and rapidity distributions at a small value of $s_{\min} = 0.001\,\mathrm{GeV}^2$, computed with T_1 only. We see the usual Jacobian peak near the kinematic maximum of the p_{T} spectrum. In Fig. 4 we plot the $s_{\min}$ dependence of the one-loop contributions to $\mathrm{d}\Gamma/p_{\mathrm{T}}$ at two fixed values of p_{T}, one halfway and the other close to the kinematic maximum. The dip in the curves is an artifact which arises because at that $s_{\min}$ and for the p_{T} given, it is no longer kinematically possible for the full phase space in Fig. 1 to contribute. Note that the dip disappears for the exact $T_1+T_2+T_3$ case. Similar results are shown for the heavy quark rapidity distributions in Fig. 5 (where we show only the positive-rapidity part of the distribution). These figures show that the freedom to choose $s_{\min}$ when including all T_i persists for distributions.

3 Dipole subtraction

In the dipole formalism one subtracts a suitable term from the real emission part and adds it again to the virtual correction after having performed one phase space integration. The subtraction term consists of a sum of dipoles, each of which can be viewed as an emitter–spectator–antenna radiating a third particle. In the case at hand, there are only two dipoles. In one of these the heavy quark constitutes the emitter with the antiquark being the spectator. The second dipole has the roles of the quark and antiquark exchanged. The matrix element to be subtracted from the real emission part reads

$$\begin{aligned}|\mathcal{M}_{\mathrm{A}}|^2 &= 2C_F g_s^2 \,|\mathcal{M}_{\mathrm{Born}}|^2 \,\frac{1}{r_0 r\sqrt{(1-r)(1-r_0 r)}}\\ &\times\left\{\frac{1}{s_{13}}\left[2(1-r_0 r)-(1-r_0)-\frac{1-r_0}{1-u_0 u}\right]\right.\\ &\left.+\;\frac{1}{s_{23}}\left[2(1-r_0 r)-(1-r_0)-\frac{1-r_0}{1+u_0 u}\right]\right\}. \quad (22)\end{aligned}$$

Here

$$\begin{aligned}&r_0=\beta^2,\quad r=\frac{s_{13}+s_{23}}{s-4m^2},\quad u_0=\sqrt{\frac{r_0(1-r)}{1-r_0 r}},\\ &u=-\frac{1}{u_0}\frac{s_{13}-s_{23}}{s_{13}+s_{23}}. \quad (23)\end{aligned}$$

This contribution is then integrated over the dipole phase space and added to the virtual corrections. The integrated version reads:

$$\begin{aligned}&\int \mathrm{dPS}_{\mathrm{dipole}}\,|\mathcal{M}_{\mathrm{A}}|^2\\ &= C_F\frac{g_s^2}{4\pi^2}\frac{1}{\Gamma(1-\varepsilon)}\left(\frac{4\pi\mu^2}{s}\right)^{\varepsilon}|\mathcal{M}_{\mathrm{Born}}|^2\\ &\times\left\{\frac{1}{\varepsilon}\left(1-\frac{1}{2}\frac{1+r_0}{\sqrt{r_0}}\ln\frac{1+\sqrt{r_0}}{1-\sqrt{r_0}}\right)\right.\\ &-2\ln r_0-\ln^2\left(\frac{1+\sqrt{r_0}}{1-\sqrt{r_0}}\right)+\frac{1}{\sqrt{r_0}}\ln\left(\frac{1+\sqrt{r_0}}{1-\sqrt{r_0}}\right)\\ &-\frac{1+r_0}{2\sqrt{r_0}}\left(\mathrm{Li}_2\left(\sqrt{r_0}\right)-\mathrm{Li}_2\left(-\sqrt{r_0}\right)\right.\\ &+2\mathrm{Li}_2\left(\frac{1+\sqrt{r_0}}{2}\right)-2\mathrm{Li}_2\left(\frac{1-\sqrt{r_0}}{2}\right)\\ &+\mathrm{Li}_2\left(\frac{\sqrt{r_0}-1}{2\sqrt{r_0}}\right)-\mathrm{Li}_2\left(\frac{\sqrt{r_0}-1}{\sqrt{r_0}}\right)\\ &+\mathrm{Li}_2\left(\frac{1}{1+\sqrt{r_0}}\right)-\mathrm{Li}_2\left(\frac{1-\sqrt{r_0}}{1+\sqrt{r_0}}\right)\\ &-2\ln r_0\ln\left(\frac{1+\sqrt{r_0}}{1-\sqrt{r_0}}\right)+\ln 2\ln\frac{\sqrt{r_0}}{1+\sqrt{r_0}}\\ &+\frac{1}{2}\ln^2 2+\ln(1-\sqrt{r_0})\ln\left(\frac{1+\sqrt{r_0}}{\sqrt{r_0}}\right)\\ &\left.\left.+\frac{1}{2}\ln^2(1+\sqrt{r_0})-\frac{1}{2}\ln^2(1-\sqrt{r_0})\right)\right\}+O(\varepsilon). \quad (24)\end{aligned}$$

The poles in ε cancel against those of the virtual corrections.

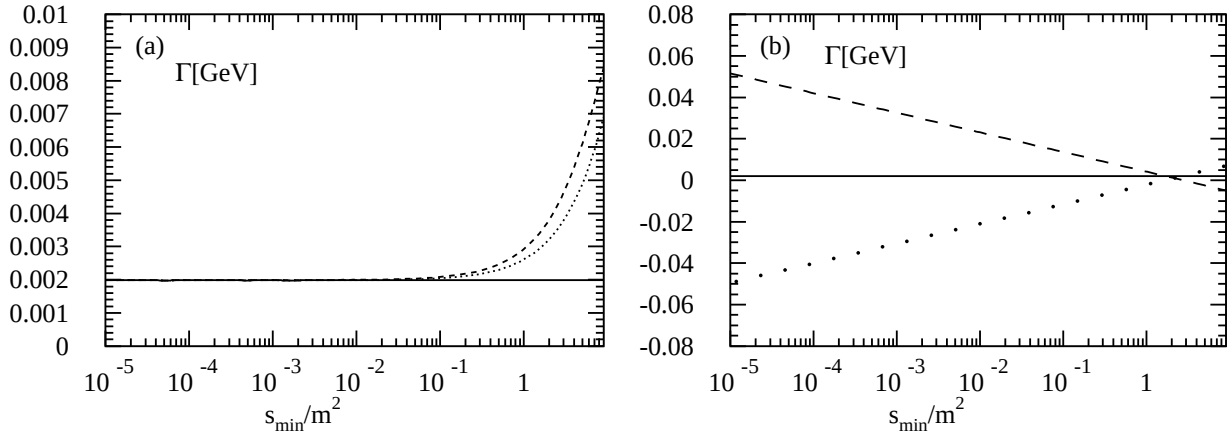

Fig. 2. **a** The $s_{\min}/m^2$ dependence of the one-loop corrections to $\Gamma(s, m^2)$, when including the T_1 (dotted), $T_1 + T_2$ (dashed), and $T_1 + T_2 + T_3$ (solid) contributions. **b** The $s_{\min}/m^2$ dependence of the one-loop corrections to $\Gamma(s, m^2)$ for the soft + virtual (spaced dotted) and the real emission (spaced dashed) final state contributions as well as their sum (solid) in the $T_1 + T_2 + T_3$ approximation

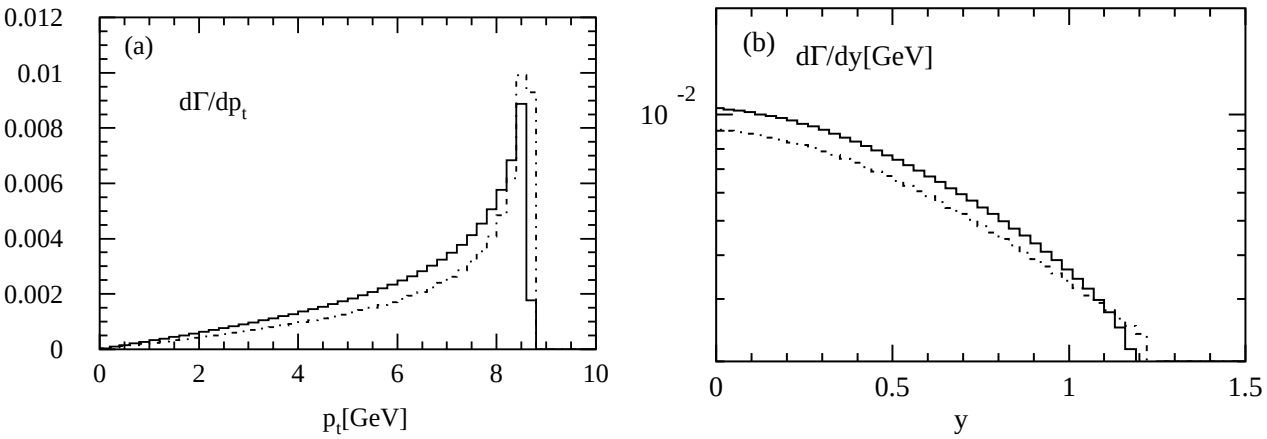

Fig. 3a,b. Differential decay widths at Born (dotted-dashed) and NLO (solid) levels, with parameters $s = 400\,\mathrm{GeV}^2$, $m = 5\,\mathrm{GeV}$, and $s_{\min} = 0.001\,\mathrm{GeV}^2$ for differential variables; (a) transverse momentum $\mathrm{d}\Gamma/\mathrm{d}p_{\mathrm{T}}$, (b) rapidity $\mathrm{d}\Gamma/\mathrm{d}y$ [GeV]

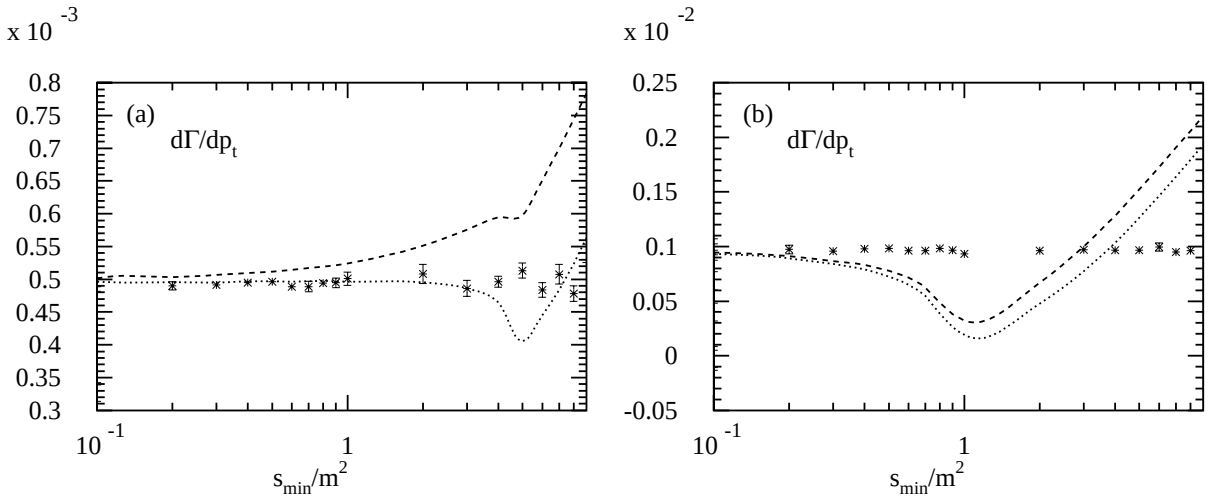

Fig. 4. **a** The $s_{\min}$ dependence of the one-loop contributions to $\mathrm{d}\Gamma/p_{\mathrm{T}}$ for $p_{\mathrm{T}} = 5\,\mathrm{GeV}$. We plot the results including the T_1 (dotted), $T_1 + T_2$ (dashed) and $T_1 + T_2 + T_3$ (individual points with error bars) terms. **b** The $s_{\min}$ dependence of the one-loop contributions to $\mathrm{d}\Gamma/p_{\mathrm{T}}$ for $p_{\mathrm{T}} = 8\,\mathrm{GeV}$. Labels as in **a**

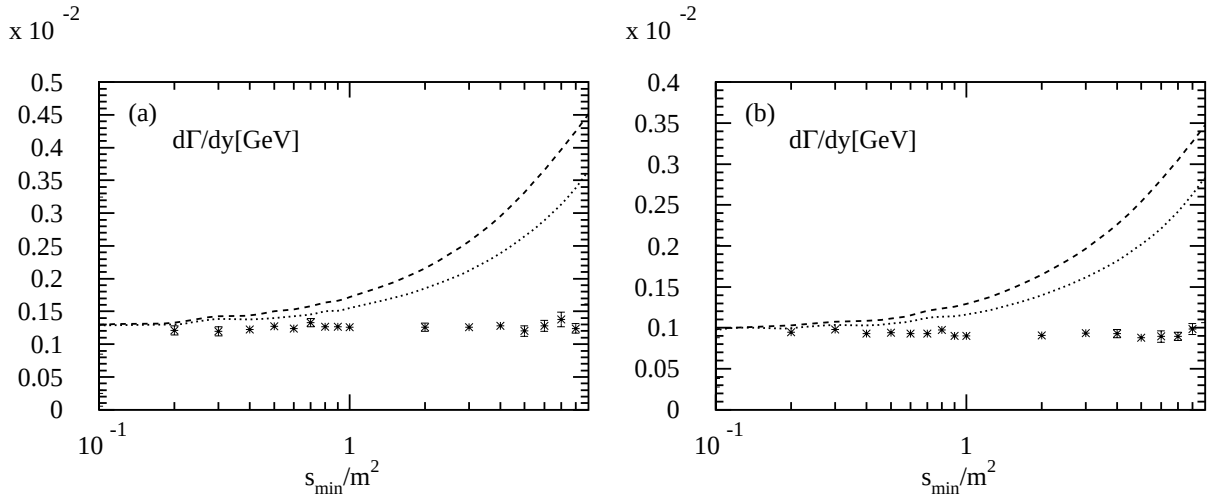

Fig. 5. **a** The $s_{\min}$ dependence of the one-loop contributions to $\mathrm{d}\Gamma/\mathrm{d}y$ at $y = 0.3$. Labels as in Fig. 4. **b** The $s_{\min}$ dependence of the one-loop contributions to $\mathrm{d}\Gamma/\mathrm{d}y$ at $y = 0.6$. Labels as in Fig. 4

We do not show separate results for the dipole method, which is exact and independent of any theoretical cut-off parameter. Numerical results for the dipole method in comparison to the PSS method can be found in the next section.

4 Comparisons of PSS and dipole subtraction

In this section we perform some numerical comparisons between the two methods for the process at hand. We use as phase space measure the expression (18). The integrations over its variables are performed using the well-known Monte Carlo iterative integration routine VEGAS [20]. We note that we found similar results when we used (17), generating the 4-vectors via a cascade algorithm. This required using more random number points in order to achieve the same accuracy.

The PSS method is relatively easy to implement, with little analytical calculation, at the expense of requiring cancellations between large numbers (for small $s_{\min}$) or having multiple negative contributions (for large $s_{\min}$ when including T_1, T_2 and T_3). Since the dipole method requires more analytical preparation work to be implemented, we expect it to show better numerical integration in the Monte Carlo program. We will see that this expectation is borne out by our results.

Our first comparison addresses the relative accuracy achieved in the computation of the inclusive cross section as a function of the number of points, for 20 iterations, of which we use the first five to set the VEGAS grid [20], leaving a sample of $N = 15$ results. For each method, we perform separate runs for the $O(\alpha_s)$ 2-particle and $O(\alpha_s)$ 3-particle contributions, and combine them for each iteration, leading to 15 results r_i. The mean result r and its error δr are then computed as

$$r = \frac{1}{N}\sum_{i=1}^{N} r_i, \quad \delta r = \sqrt{\frac{1}{N}\frac{\sum_{i=1}^{N}(r_i - r)^2}{N-1}}. \qquad (25)$$

Table 1. Accuracy $\delta r/r$ of the inclusive cross section attained for a given number of points per iteration in the two methods. The same phase space and random number generators are employed. The PSS results use the T_1 contribution only, with $s_{\min} = 0.001\,\mathrm{GeV}^2$

$s = 400\,\mathrm{GeV}^2$		
points	DIP	PSS
1000	0.04%	1%
10000	0.009%	0.3%
100000	0.003%	0.1%

Table 2. Comparison of the two methods as to the approximate relative deviations of their first three (grid-setting) iterations from the final mean (computed starting from the fifth iteration), for the case of the inclusive cross section. The same phase space and random number generators are employed, at $s = 400\,\mathrm{GeV}^2$. The PSS results use the T_1 contribution only, with $s_{\min} = 0.001\,\mathrm{GeV}^2$

iteration	DIP	PSS
1	0.1%	100%
2	0.09%	70%
3	0.06%	10%

The results for this comparison are given in Table 1. We note that the PSS method suffers further penalties in accuracy and efficiency if the value of $s_{\min}$ is chosen so large that the T_2 and T_3 become necessary; in particular the T_3 contribution requires generating the soft phase space measure, and involves the difference of two phase space measures which are very similar in magnitude for small values of the soft invariants, cf. (7).

Our second comparison addresses the efficiency in the computation of the inclusive cross section as a function of the number of iterations, for 10^4 random number points.

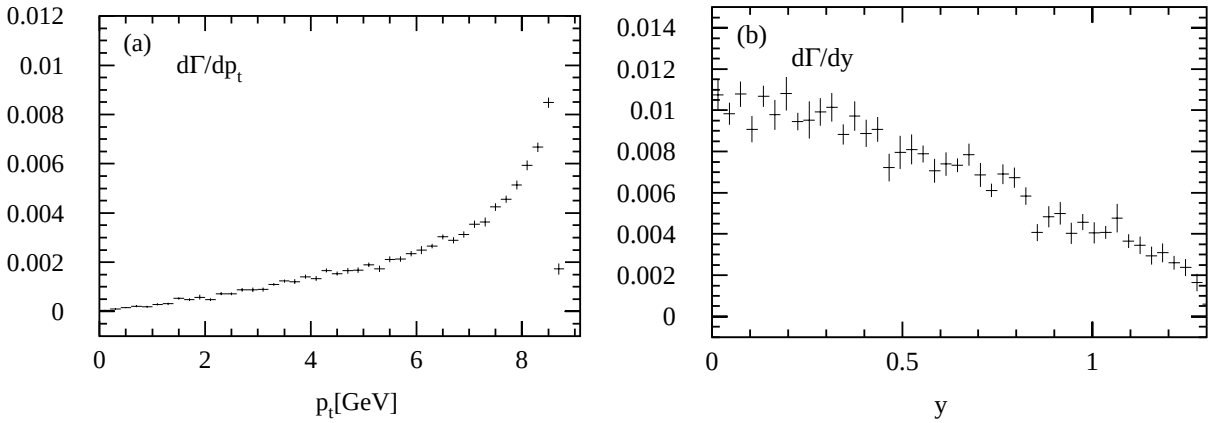

Fig. 6a,b. Differential decay widths at NLO level, with parameters $s = 400\,\mathrm{GeV}^2$, $m = 5\,\mathrm{GeV}$, for the phase space slicing method (at $s_{\min} = 0.001\,\mathrm{GeV}^2$) for differential variables; **a** transverse momentum $\mathrm{d}\Gamma/\mathrm{d}p_{\mathrm{T}}$, **b** rapidity $\mathrm{d}\Gamma/\mathrm{d}y$ [GeV]

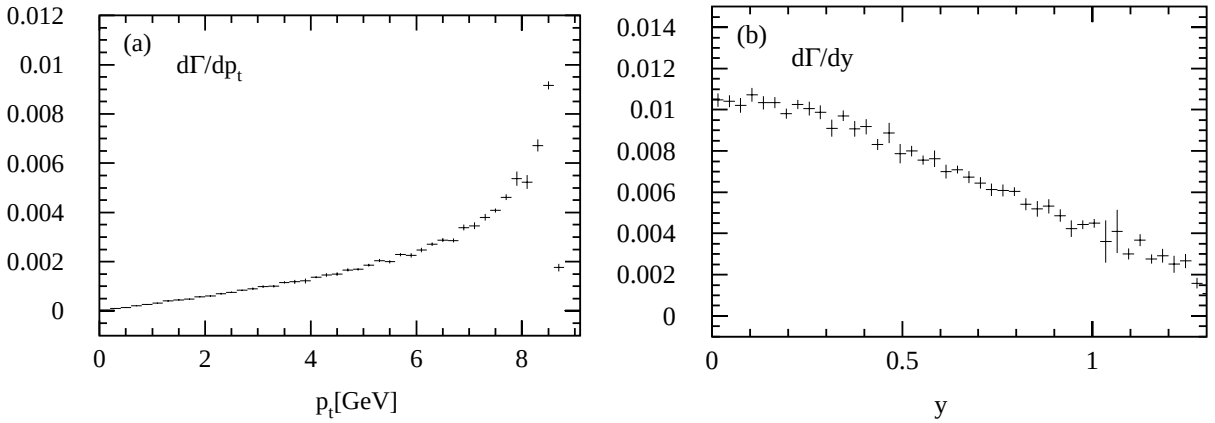

Fig. 7a,b. Differential decay widths at NLO level, with parameters $s = 400\,\mathrm{GeV}^2$, $m = 5\,\mathrm{GeV}$, for the dipole method for differential variables; **a** transverse momentum $\mathrm{d}\Gamma/\mathrm{d}p_{\mathrm{T}}$, **b** rapidity $\mathrm{d}\Gamma/\mathrm{d}y$ [GeV]

We see that the dipole method reaches a given accuracy with less iterations.

Next we compare the efficiency of these methods to compute transverse momentum and rapidity distributions. As before, the first 5 of 20 iterations are used solely for grid-setting, with 10^4 points per iteration. The values and their errors for each bin are computed according to (25). We see that the dipole methods produces somewhat smaller errors, with slightly less bin to bin variations. When we increased the number of points, we saw that both methods perform not too differently. We also noticed that this loss of superiority is progressive with the number of bins. This suggests that parts of the positive and negative contributions end up in different bins. To test this idea, we performed a simple smearing where each event with weight w that would normally end up in bin i is distributed in bins $i-1, i, i+1$, each with weight $w/3$. We found that this smearing indeed reduced the errors somewhat, but in about equal measure for both methods.

Finally, we compared the accuracies of the methods in the large s limit for the inclusive cross section, where the heavy quarks become effectively massless. For the PSS method we investigated how to choose $s_{\min}$ in order to minimize the calculation error. We found that $s_{\min}$ is best chosen not too small (which would lead to large numerical cancellations), and as a fraction of s between 0.01 and 0.1. For large $s_{\min}$ this may require the inclusion of the T_2 and T_3 terms, which contribute about 10% to the cross section for $s_{\min} = 0.1s$ at $s = 250000\,\mathrm{GeV}^2$. For $s = 250000\,\mathrm{GeV}^2$ and $s_{\min} = 0.01s$ their contribution is only 2%, with a slightly larger total error for the same number of points. We found similar results keeping s fixed and letting m become smaller. For the dipole method we found that it has consistently better accuracy than the PSS method in these limits. In general in the high-energy limit, both these methods lead to cancellations between contributions with $+\ln(s/m^2)$ and $-\ln(s/m^2)$ terms, which is not advantageous numerically. Therefore a method which avoids such logarithms could be desirable [18].

5 Conclusions

In this paper we have compared the accuracy and efficiency of two general-purpose methods to compute NLO heavy quark production cross sections, for a very simple

case. We found the dipole method [12,13], while involving additional analytical work, to be superior in efficiency and accuracy. A similar conclusion was reached by Dittmaier [14] who compared his method with a slicing calculation for a number of electroweak cross sections.

The phase space slicing method [8–10], which is easy to use and minimizes analytical work, can be extended [19] to become fully independent of the slicing parameter, which we demonstrated in this paper for the reaction at hand. Although our case study involves only the simplest of heavy quark production processes, it is, we believe a useful first step toward gaining numerical experience with general methods for constructing NLO Monte Carlo programs for heavy quark production. Moreover, such experience gained at NLO is likely to be very valuable when these methods are generalized for NNLO cross sections.

Acknowledgements. The work of T.O.E., E.L. and L.P. is supported by the Foundation for Fundamental Research of Matter (FOM) and the National Organization for Scientific Research (NWO).

Appendix A: A subtlety in phase space slicing

In this appendix we mention a subtlety in implementing PSS, which is well known to experts in the field, but not readily found in the literature. It does not come into play for our simple case study, but does for amplitudes in which more than one color structure is present. The correct implementation of phase space slicing requires that the real emission amplitude be decomposed into pieces with a unique singularity structure and that the slicing procedure be defined for each piece separately.

We discuss the point for a simplified example, where we take al particles to be massless. We assume that the real emission amplitude is given by

$$|\mathcal{M}_4|^2 = \frac{1}{s_{13}s_{34}s_{24}} + \frac{1}{s_{14}s_{34}s_{23}}. \tag{A.26}$$

This simple example has the singularity structure for the leading-color part of the $\gamma^* \to q\bar{q}gg$ amplitude. The correct way to implement phase space slicing treats each singularity structure separately and the resolved contribution from the real emission amplitude reads therefore

$$\begin{aligned}&\int \mathrm{dPS}_4 \frac{1}{s_{13}s_{34}s_{24}} \theta(s_{13} - s_{\min})\,\theta(s_{34} - s_{\min}) \\ &\quad \times\theta(s_{24} - s_{\min}) \\ &+ \int \mathrm{dPS}_4 \frac{1}{s_{14}s_{34}s_{23}} \theta(s_{14} - s_{\min})\,\theta(s_{34} - s_{\min}) \\ &\quad \times\theta(s_{23} - s_{\min})\,.\end{aligned} \tag{A.27}$$

The incorrect method cuts out all possible singularities from the amplitude and uses the expression

$$\begin{aligned}&\int \mathrm{dPS}_4 \left(\frac{1}{s_{13}s_{34}s_{24}} + \frac{1}{s_{14}s_{34}s_{23}}\right) \theta(s_{13} - s_{\min}) \\ &\quad \times\theta(s_{34} - s_{\min})\,\theta(s_{24} - s_{\min}) \\ &\quad \times\theta(s_{14} - s_{\min})\,\theta(s_{23} - s_{\min})\end{aligned} \tag{A.28}$$

for the resolved contribution. The difference between the correct implementation and the incorrect one consists of terms of the form

$$\begin{aligned}&\int \mathrm{dPS}_4 \frac{1}{s_{13}s_{34}s_{24}} \theta(s_{13} - s_{\min}) \\ &\quad \times\theta(s_{34} - s_{\min})\,\theta(s_{24} - s_{\min}) \\ &\quad \times\theta(s_{\min} - s_{14})\,\theta(s_{23} - s_{14})\,,\end{aligned} \tag{A.29}$$

together with three similar terms, obtained by exchanging $3 \leftrightarrow 4$ in the matrix element and the slicing procedure. Contrary to naive expectations, these terms do not vanish in the limit $s_{\min} \to 0$, but give a constant contribution.

References

1. K. Fabricius, I. Schmitt, G. Kramer, G. Schierholz, Zeit. Phys. C **11**, 315 (1981)
2. G. Kramer, B. Lampe, Fortschr. Phys. **37**, 161 (1989)
3. H. Baer, J. Ohnemus, J.F. Owens, Phys. Rev. D **40**, 2844 (1989)
4. B.W. Harris, J.F. Owens (2001), hep-ph/0102128
5. R.K. Ellis, D.A. Ross, A.E. Terrano, Nucl. Phys. B **178**, 421 (1981)
6. Z. Kunszt, P. Nason, G. Marchesini, B.R. Webber, Proceedings of the 1989 LEP Physics Workshop, Geneva, edited by G. Altarelli, R. Kleiss, C. Verzegnassi, vol. 1, p. 373
7. M.L. Mangano, P. Nason, G. Ridolfi, Nucl. Phys. B **373**, 295 (1992)
8. W.T. Giele, E.W.N. Glover, Phys. Rev. D **46**, 1980 (1992)
9. W.T. Giele, E.W.N. Glover, D.A. Kosower, Nucl. Phys. B **403**, 633 (1993), hep-ph/9302225
10. S. Keller, E. Laenen, Phys. Rev. D **59**, 114004 (1999), hep-ph/9812415
11. S. Frixione, Z. Kunszt, A. Signer, Nucl. Phys. B **467**, 399 (1996), hep-ph/9512328
12. S. Catani, M.H. Seymour, Nucl. Phys. B **485**, 291 (1997), hep-ph/9605323
13. L. Phaf, S. Weinzierl, JHEP **04**, 006 (2001), hep-ph/0102207
14. S. Dittmaier, Nucl. Phys. B **565**, 69 (2000), hep-ph/9904440
15. J.M. Campbell, M.A. Cullen, E.W.N. Glover, Eur. Phys. J. C **9**, 245 (1999), hep-ph/9809429
16. L. Reina, S. Dawson (2001), hep-ph/0107101
17. W. Beenakker et al. (2001), hep-ph/0107081
18. S. Catani, S. Dittmaier, M. Seymour, Trócsányi, in preparation
19. W.B. Kilgore, W.T. Giele, Phys. Rev. D **55**, 7183 (1997), hep-ph/9610433
20. G.P. Lepage, J. Comput. Phys. **27**, 192 (1978)